Contribution 4

A common solution to the R_D anomalies and Dark Matter

G. Bélanger, J. Bernigaud, A. Bharucha, B. Fuks, A. Goudelis, J. Heisig, A. Jueid, A. Lessa, D. Marzocca, M. Nardecchia, G. Polesello, P. Pani, A. Pukhov, D. Sengupta and J. Zurita

Abstract

The anomalies observed by LHCb in flavor observables suggest the breakdown of lepton flavor universality. We study how a vanilla leptoquark solution to the $R_{D^{(*)}}$ anomalies can also explain the measured relic abundance, if the leptoquark mediates between the visible sector and the dark sector.

1 Introduction

The current LHC dataset has not shown any significant deviation from the Standard Model (SM) expectations, except for the $R_{K^{(*)}}$ [33, 34] and $R_{D^{(*)}}$ [35–37] anomalies. While many models have been considered to explain these observations, the consensus is that two classes of models can accommodate these results: leptoquarks and Z' models (for a recent review see e.g [38] and references therein). It is thus interesting to consider the interplay between these solutions and dark matter (DM), which requires to allow an additional decay of the leptoquark into the dark sector, studied previously in [39, 40]. As this will reduce the branching ratios of the visible decays of the leptoquarks, it naively allows one to lower the current constraint on $m_{LQ} \gtrsim 1$ TeV with $\mathcal{O}(1)$ couplings, thus opening up novel parameter space and increasing the opportunities to probe this model at the LHC in the near future.

For our study we built a simplified model featuring the minimal ingredients to explain the charged current flavor anomalies $R_{D^{(*)}}$ and dark matter simultaneously, limiting ourselves to the couplings strictly necessary to explain the anomaly. We study how the different phenomenological constrains affect the parameter space: LHC searches for leptoquarks and dark matter, relic density, direct and indirect detection. We pay particular attention to the existing CMS search for a resonant leptoquark plus missing energy [41]: while this search might not always be the golden channel for discovery, its importance lies in the fact that this is the only channel probing the $R_{D^{(*)}}$-DM connection (RDM).

2 The model

We consider a simplified model in which we supplement the Standard Model by one scalar leptoquark field S_1 and two extra fermionic fields, a Majorana fermion χ_0 and a Dirac fermion χ_1. The S_1 and χ_1 fields are electrically-charged coloured weak singlets lying in the $(\mathbf{3}, \mathbf{1})_{-1/3}$ representation of the Standard Model gauge group. In contrast, χ_0 is a dark matter candidate and therefore a non-coloured electroweak singlet. In our FEYNRULES [18] implementation, we consider all potential interactions of the new sector with the Standard Model sector, the corresponding Lagrangian being written as

$$\mathcal{L} = \mathcal{L}_{\rm SM} + \mathcal{L}_{\rm kin} + \bigg[\lambda_{\bf R}\, \bar{u}_R^c\, \ell_R\, S_1^\dagger + \lambda_{\bf L}\, \bar{Q}_L^c \!\cdot\! L_L\, S_1^\dagger + y_\chi \bar{\chi}_1 \chi_0 S_1 + {\rm h.c.}\bigg] \ . \qquad (1)$$

In this expression, all flavour indices are understood for simplicity and the dot stands for the $SU(2)$-invariant product of two fields lying in the fundamental representation. In addition, $\mathcal{L}_{\rm SM}$ is the Standard Model Lagrangian and $\mathcal{L}_{\rm kin}$ contains gauge-invariant kinetic and mass terms for all new fields, the χ_1 state being assumed vector-like. The Q_L and L_L spinors stand for the $SU(2)_L$ doublets of left-handed quarks and leptons respectively, whilst u_R and ℓ_R stand for the $SU(2)_L$ singlets of right-handed up-type quarks and charged leptons, respectively. The $\lambda_{\rm L}$ and $\lambda_{\rm R}$ couplings are 3×3 matrices in the flavour space, that are considered real in the following. Moreover, in our conventions, the first index i of any λ_{ij} element refers to the quark generation whilst the second one j refers to the lepton generation.

The field content of the new physics sector of our simplified model is presented in table 1, together with the corresponding representation under the gauge and Poincaré groups, the potential Majorana nature of the different particles, the adopted symbol in the FeynRules implementation and the PDG identifier that has been chosen for each particle. The new physics coupling parameters are collected in table 2, in which we additionally include the name used in the FeynRules model and the Les Houches blocks [42] in which the numerical values of the different parameters can be changed by the user when running tools like MG5_aMC [43] or MicrOMEGAs [44].

Field	Spin	Repr.	Self-conj.	FeynRules name	PDG code
S_1	0	$(\mathbf{3},\mathbf{1})_{-1/3}$	no	`LQ`	42
χ_0	1/2	$(\mathbf{1},\mathbf{1})_0$	yes	`chi0`	5000521
χ_1	1/2	$(\mathbf{3},\mathbf{1})_{-1/3}$	no	`chi1`	5000522

Table 1: *New particles supplementing the Standard Model, given together with the representations under $SU(3)_c \times SU(2)_L \times U(1)_Y$. We additionally indicate whether the particles are Majorana particles, their name in the* FeynRules *implementation and the associated Particle Data Group (PDG) identifier. Note that the PDG code 42 is the official PDG value for our leptoquark [45] and hence there are no issues when running showering and/or hadronizing the event sample.*

Coupling	FeynRules name	Les Houches block
$(\lambda_L)_{ij}$	`lamL`	`LQLAML`
$(\lambda_R)_{ij}$	`lamR`	`LQLAMR`
y_χ	`yDM`	`DMINPUTS`

Table 2: *Couplings of the new particles, given together with the associated* FeynRules *symbol and the Les Houches block of the parameter card.*

In a nutshell, our model needs three new masses and several new couplings.The R_D

anomalies can be explained with only non-zero $(\lambda_L)_{33} \equiv \lambda_L$[1] and $(\lambda_R)_{23} \equiv \lambda_R$. Finally, the dark matter phenomenology requires the coupling y_χ. Hence these 6 parameters span our parameter space. In what follows we will study how the flavor anomalies, dark matter phenomenology and collider searches constrain the parameter space of this model, showing the currently allowed regions and commenting on the future prospects.

3 Leptoquark solutions to the R_D anomalies

As mentioned in the previous chapter, a minimal solution of the $R_{D^{(*)}}$ anomalies can be obtained with just a left-handed ($(\lambda_L)_{33}$) and a right-handed ($(\lambda_R)_{23}$) couplings to S_1. We note that the ($(\lambda_L)_{33}$) coupling is forced to be left-handed due to the presence of the neutrino[2]. The choice of having a non-vanishing ($(\lambda_R)_{23}$) is due to the large contributions that $(\lambda_L)_{23}$ would generate to the $B \to X_s \nu\nu$ process, which could only be reduced by extending the model, e.g: considering a destructive interference with another leptoquark state [24, 25, 47, 48]. We perform a global fit of the model with the two couplings $(\lambda_L)_{33}$ and $(\lambda_R)_{23}$ as free parameters. The relevant observables included in the fit are: R_D, R^*_D, Br$(B_c \to \tau\nu)$, deviations in the Z couplings to τ_L and τ_R, effective number of neutrinos from Z decays, lepton flavour universality tests in τ decays. For more details on this fit see e.g. [24, 25, 46]. A contribution to $D^0 - \bar{D}^0$ mixing is generated at one loop, but is strongly CKM-suppressed and does not provide a relevant constraint. The results of a scan in the two parameters of the model, for $m_{S_1} = 1.5$ TeV, where all points are within 1σ of the best-fit point, is shown in the plane of the R_D and R^*_D anomalies in the left panel of figure 1. The corresponding preferred region is presented in the right panel of figure 1 in the x, y plane, with $x = \lambda_L(\text{TeV}/m_{S_1})$ and $y = \lambda_R(\text{TeV}/m_{S_1})$. [3]

From the figure we can establish two working points. We pick the first one to obtain the lowest possible $BR(S_1 \to c\tau)$, which corresponds to $(x, y) = (0.6, 0.5) = P_1$. For the second one we do not want to pick extreme values of λ_R, as we could spoil the validity of the narrow-width approximation for the leptoquark, as well as pertubativity. So we restrict ourselves to the best fit point $(0.16, 2.0) = P_2$ that already gives a negligible branching fraction into the third generation states. We thus use these working points to generate concrete benchmarks by picking two values for the leptoquark mass: $m_{S_1} = 500$ GeV and $m_{S_1} = 1000$ GeV. We show the corresponding values of the couplings and branching ratios in Table 3, where we have assumed a negligible coupling of S_1 to the dark sector. We note that the solution of the $R_{D^{(*)}}$ anomalies, being an off-shell interference with the SM amplitude, will not be affected by diluting the leptoquark visible decays, but it would rather loose the constraints coming from direct searches of S_1, which we discuss in detail in Section 4.

Before starting with the relevant collider and dark matter phenomenology, it is instructive to take a further insight into the phenomenology of our benchmarks. In figure 2 we show the branching fractions of S_1 and χ_1 for each of our working points, setting $m_{S_1} = 1$ TeV. For concreteness we fixed the dark coupling $y_{DM} = 0.2$ and $\Delta = m_{\chi_1} - m_{\chi_0} = 100$ GeV, but the phenomenology does not strongly depend on the actual values. Note that in our model the χ_1 always decays into a 3-body final state via an intermediate S_1. The phenomenology for the second case (right panel) is fairly simple: the dominant decay of S_1 is into a charm-quark

[1] The second index is not constrained, as the neutrino flavor is not tagged. For simplicity we restrict it here to the third generation.

[2] Alternatively one could explicitly introduce a right-handed neutrino that could serve as a dark matter candidate, see e.g [46].

[3] The $R_{D^{(*)}}$ anomalies scale with the product xy, while other constraints scale instead with x^2 or y^2.

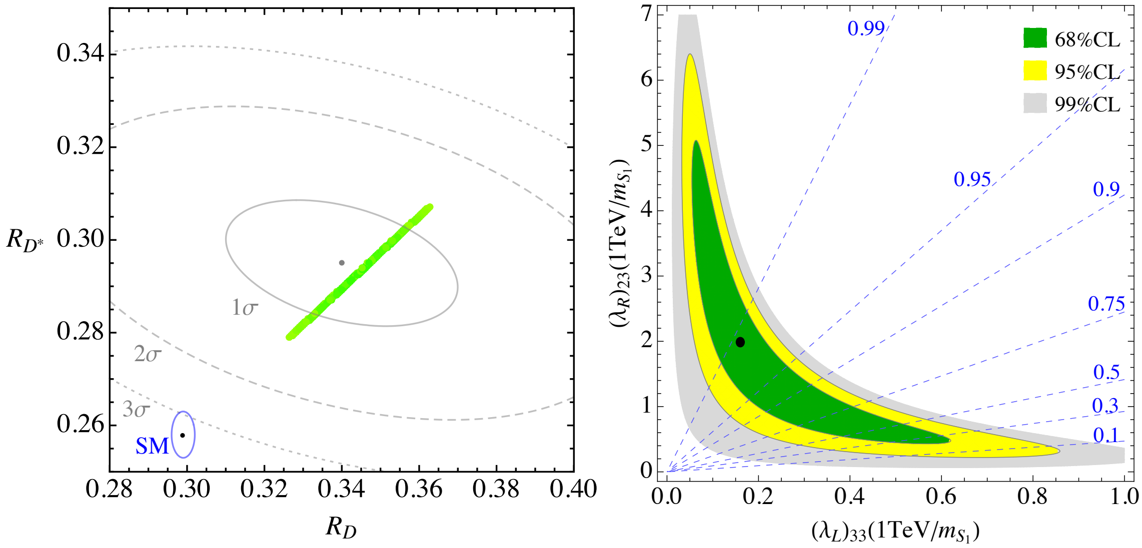

Figure 1: *Left: flavor fit to the charged current anomalies for* $m_{S_1} = 1.5$ *TeV (*1σ *region). The gray lines represent the present status in the measurements of the two observables, compared with the SM point (blue point and contour). Right: Viable parameter space from the fit of flavor and precision observables as function of* λ/m_{S_1}*. Blue dashed lines are iso-lines of the branching ratio* $B(S_1 \to c_R \tau_R)$ *assuming* $y_\chi \ll (\lambda_L)_{33}, (\lambda_R)_{23}$ *and* $m_{S_1} \gg m_t$*. The black dot represents the best-fit point.*

m_{S_1} [GeV]	λ_L	λ_R	$BR(S_1 \to b\nu)$	$BR(S_1 \to t\tau)$	$BR(S_1 \to c\tau)$	$\Gamma(S_1)/m_{S_1}$
500	0.30	0.25	0.4049	0.3139	0.2812	4.42E-3
1000	0.6	0.5	0.3794	0.3571	0.2635	1.89E-2
500	0.08	1.0	0.0063	0.0049	0.9887	3.4E-2
1000	0.16	2.0	0.0063	0.0059	0.9877	8.06E-2

Table 3: Benchmark points compatible with the flavour anomalies. Here we have assumed negligible decays into the dark sector. Note the wide range of possibilities for the $c - \tau$ channel (from 25 % to roughly 100%) while the b and top decays have an upper bound of about 40 and 30 % respectively, and can actually become at the sub-percent level.

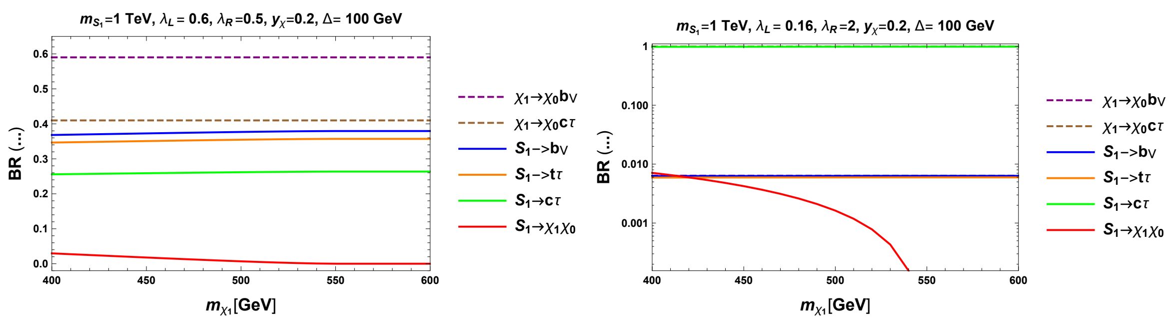

Figure 2: Branching ratios (top) for the S_1 and χ_1 as a function of the χ_1 mass. The mass difference between χ_1 and χ_0 is kept as 100 GeV, $y_\chi = 0.2$ and the other parameters correspond the second and fourth line of Table 3, called P_1 and P_2 in the main text.

and a tau-lepton, hence χ_1 decays via an off-shell S_1 almost exclusively into $c\,\tau\,\chi_0$. In the first scenario, where λ_L and λ_R are comparable, S_1 decays with appreciable ratios into both the three “visible" channels and the invisible one. As a consequence, χ_1 decays into the $c\,\tau\chi_0$ and $b\nu\chi_0$ final states with similar ratios while the top final state is kinematically closed. This information is not enough to anticipate the collider phenomenology, as we will also need the production cross sections for S_1 and χ_1 states. We present the leading-order (LO) QCD cross sections as a function of m_{χ_1} and m_{S_1} in figure 3 for the three main production processes: pair production of S_1 and χ_1 via gauge interactions, and associated production of a leptoquark and a tau-lepton. We have used as a benchmark the fourth line from Table 3, hence when scanning over m_{S_1} we also vary $\lambda_{L,R}$ as to keep x and y fixed to the benchmarked values.

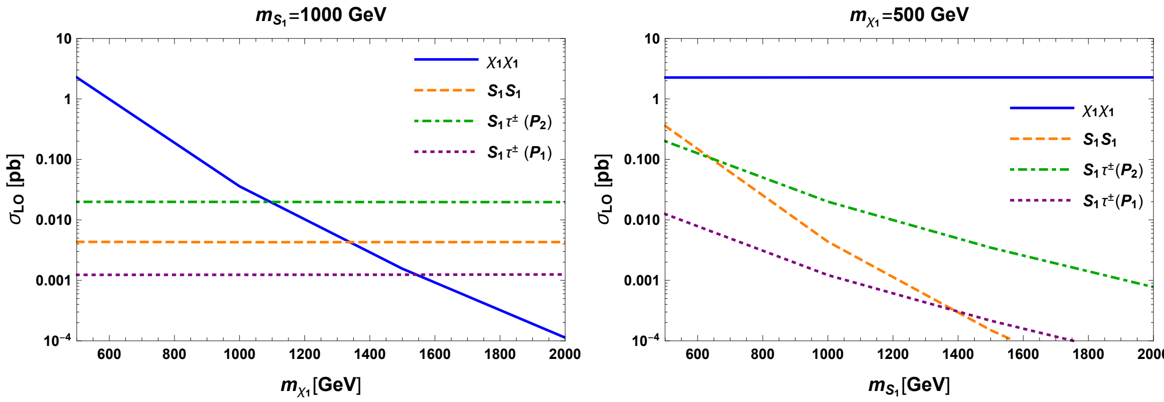

Figure 3: Cross-sections for S_1 and χ_1 production at the LHC as a function of m_{χ_1} (left panel) and m_{S_1} (right panel), for pair production of χ_1 (solid blue), pair production of S_1 (dashed orange) and associated production of S_1 and a tau lepton, which is shown for the benchmark points P_2 (dot-dashed green) and P_1 (dotted green). In the right panel we kept fixed $x = \lambda_L \mathrm{TeV}/m_{S_1}$ and $y = \lambda_R \mathrm{TeV}/m_{S_1}$ to the corresponding P_1 and P_2 values, see main text for details.

.

It comes as no surprise that the pair production of χ_1 is the process with the largest cross section, as both S_1 and χ_1 have the same colour charges but χ_1 is a fermion, and also because we are assuming that $S_1 \to \chi_1\chi_0$ occurs on-shell, hence χ_1 is lighter than S_1[4]. The single LQ cross section becomes relevant for large values of λ_R: the $S_1\tau$ cross section intercepts S_1 pair production at about 700 GeV (1.4 TeV) for $P_1(P_2)$, while the S_1 pair production cross section gets suppressed very fast by the large-x parton distribution functions. In the case of P_1, where λ_L and λ_R are comparable, then we should also include associated production of S_1 with bottom and top quarks, but these are PDF suppressed and give a negligible contribution to the total cross section at the LHC. These could however be important when considering future hadron colliders with larger energies [49].

4 LHC constraints

Our model contains three new fields that are probed by several LHC searches, which generically fall into two categories. On one hand, we have direct searches for leptoquarks (S_1), both for single and double production. On the other hand we have the full spectrum of missing transverse energy (MET) searches targeting invisible final states, in our case driven by pair production of χ_1 via gauge interactions. As a hybrid of both categories, the CMS search for leptoquark

[4]If we abandon this hypothesis the take-home message is exactly the same: the largest event rate corresponds to the lightest BSM colored particle in the spectrum.

plus dark matter [41], inspired by the Coannihilation Codex [40], gives not only interesting constraints on the parameter space, but moreover it would allow us to establish the connection between the flavor anomalies and dark matter, in a post-discovery scenario.

In each of the categories described above, we will consider both a) existing searches and b) novel searches (for instance, the aforementioned LQ + MET search of ref [41] only applies if the leptoquark decays to muons, but it is not applicable for e.g: electron decays). Given the large number of searches and the many processes they target, we summarize the ones we will use in this section in Table 4.

Category	Reference	Target process	Remarks
LQ	[32]	$S_1 S_1 \to t\tau t\tau$	
	[32]	$S_1 S_1 \to b\nu b\nu$	
	[50]	$S_1 S_1 \to c\tau c\tau$	Recasting of $b\tau b\tau$ study.
	Buttazzo et al. this volume	$S_1 S_1 \to b\nu t\tau$	
	[23]	$S_1 \tau \to c\tau\tau$	Rescaling of $b\tau\tau$ study
MET	[51,52]	$\chi_1\chi_1 \to bb\chi_0\chi_0$	
	[53]	$\chi_1\chi_1 \to \tau\tau\chi_0\chi_0$	
	[54]	$\chi_1\chi_1 \to \chi_0\chi_0 + nj$	$n \geq 2$ only.
	[55]	$\chi_1\chi_1 \to \chi_0\chi_0 + nj$	$1 \leq n \leq 4$
LQ + MET	[41]	$S_1 S_1 \to lq\chi_1\chi_0$	CMS requires μ, we use $\tau \to \mu$ for interpretation

Table 4: *List of searches considered in this work. We split the studies in three categories, depending if they correspond to standard leptoquark searches, MET searches, and also the CMS search for a resonant LQ + MET, belonging to the hybrid of the two first categories.*

As anticipated in the previous section, the collider bounds will be dominated by χ_1 pair production, hence we expect the $b\bar{b}$ + MET and $\tau\tau$ + MET searches to set tight constraints on the parameter space. These would lose stem as the final state becomes inefficient (e.g: in our second working point the branching ratio of $S_1 \to b\nu$ is negligible) or if the dark sector becomes compressed, giving rise to soft decay products that would not pass the reconstruction requirements. In that case we can expect a bound from the mono-jet search, where χ_1 gives only rise to MET and one invokes initial state radiation to boost the $\chi_1\chi_1$ system while allowing for an efficient trigger. This bound should however, be looser than the one from the $b\bar{b}/\tau\tau$ + MET and hence the LQ searches become competitive in probing the parameter space. The hybrid search is necessary to fingerprint the connection between the flavour anomalies and the dark sector, but naively we would not expect it to set the leading bounds.

4.1 Leptoquark searches

There are two different production mechanisms for leptoquarks at the LHC, which are shown in figure 4: pair production (left panel) due to gauge interactions[5] and single production in association with a SM fermion (right panel). The pair production is a guaranteed mode, since its cross section is only a function of the leptoquark mass. The single production cross section depends both on the leptoquark couplings to the SM fermions and with the leptoquark masses.

[5]In principle also t-channel leptonic exchange can be relevant given the size of the leptoquark couplings, and would be taken into account in the next-to-leading order calculation in a future publication.

The experimental searches for leptoquarks are organized by these production mechanisms, and we will follow the same taxonomy here.

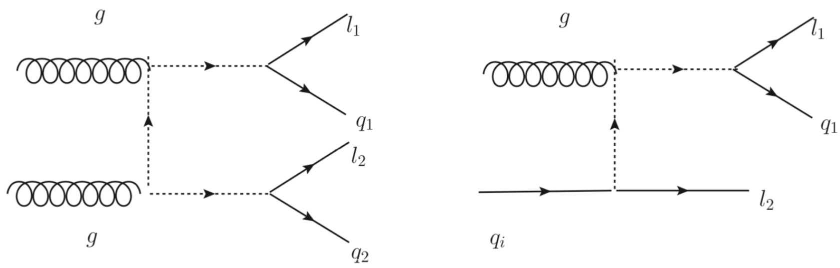

Figure 4: Representative Feynman diagrams for pair (left) and single (right) leptoquark production at hadron colliders.

4.1.1 LQ pair searches

Searches for visible decays of LQ pairs at ATLAS [32, 56, 57] and CMS [58–60], focus on both leptoquarks decaying in the same final state. In Ref. [32] five different searches are described. The first one is a search for LQ decaying into the $b\tau b\tau$ final state, reoptimising an existing di-Higgs search in the same final state [61], to the different final state kinematics. The other four searches are reinterpretations of existing studies of supersymmetric particles: searches for stop pair production in the zero-lepton [62] and one-lepton channel [63] ($t\bar{t}+$ MET), stop decays into staus [50] and a sbottom search [64] ($b\bar{b}+$ MET). Our model has four leptoquark decay channels, three into SM particles and one into the DM mediator, as shown in figure 2. Two of the decay channels are directly covered by the ATLAS searches, namely the decays into $t\tau$ and into $b\nu$, through the searches respectively for the $b\tau b\tau$ final states, and for $b\bar{b}+$ MET. For any choice of the coupling, and barring effects from the top mass, we would have that $BR(S_1 \to t\tau) \approx BR(S_1 \to b\nu)$, in contrast to the ATLAS study where $BR(S_1 \to b\nu) = 1 - BR(S_1 \to t\tau)$ is assumed.

We note that even if this search is restricted to the third generation final states, there is no search for the "mixed" final state, namely $b\nu t\tau$. In order to achieve an optimal coverage this channel should be included, and we have indeed carried out a preliminary simulation study. A detailed analysis of this final state for a 14 TeV LHC based on a parametrised simulation of the ATLAS detector, with full consideration of all relevant backgrounds is described elsewhere[6]. In this study a dedicated selection is developed to separate the final state of interest from the overwhelming $t\bar{t}$ background through novel variables which optimally exploit the kinematical features of leptoquark pair production, and its difference from the $t\bar{t}$ kinematics.

In addition we also try to address the $c\tau c\tau$ final state through a rough rescaling of the existing ATLAS $b\tau b\tau$ limits. [7]

[6]See Buttazzo et al. in the same proceedings volume.

[7]To be fully comprehensive one should also consider the mixed final states $c\tau b\nu$ and $c\tau t\tau$, but these are beyond the scope of this work. We expect them to be subdominant: given the lesser quality of c-tagging with respect to bottom- and top-tagging, c final states will only matter when the 3rd generation branching fraction is very small, $\mathcal{O}(5\%)$. In that case the largest branching fraction would occur in the $c\tau c\tau$ channel, which would be at least about an order of magnitude above the "mixed" rate.

In the model under consideration this decay is dominant over a large part of the parameter space allowed by the consideration of the flavour anomalies, as shown in figure 1, where dashed blue lines represent the isovalues of $BR(S_1 \to c\tau)$ in the $\lambda_L - \lambda_R$ plane. This final state is not targeted by the ATLAS searches which are focused on the third generation.

In absence of a dedicated analysis, a rough evaluation of the coverage for the $c\tau c\tau$ final state can be obtained by the consideration of the ATLAS results for the $b\tau b\tau$ final state. The experimental algorithm for tagging the b-jets used in Ref. [32] has an average efficiency for tagging a jet from the fragmentation of a b-quark of 70%. The same algorithm tags the jet from the fragmentation of a c-quark with an efficiency of $\sim$ 8% ([65]). Therefore the results for the $b\tau b\tau$ final can be recasted for the $c\tau c\tau$ final state by scaling down the excluded branching fraction by a factor ~8.5. This scaling is conservative, as it assumes that the analysis requires two b-tagged jets in the event, whereas both events with 1 and 2 b-tags are considered in [32]. A dedicated analysis, based on e.g. the c-tagging algorithms recently developed by ATLAS [66] should provide a much better coverage for the $c\tau$-dominated region and the inclusion of such a study within the leptoquark search programme should be high in the list of priorities of the experimental collaborations.

Both for the proposed mixed analysis and for the $c\tau c\tau$ rescaling of the ATLAS $b\tau b\tau$ analysis we evaluated, for each point in the $\lambda_L - \lambda_R$ plane the excluded mass based on the considerations above. The result is shown in figure 5, where the results for the mixed ($c\tau c\tau$) analyses are shown in the left (right) panel. For the uncovered points in the two panels the exclusion on the S_1 mass is below 400 GeV, which is the lowest mass for which the two considered analyses provide an exclusion.

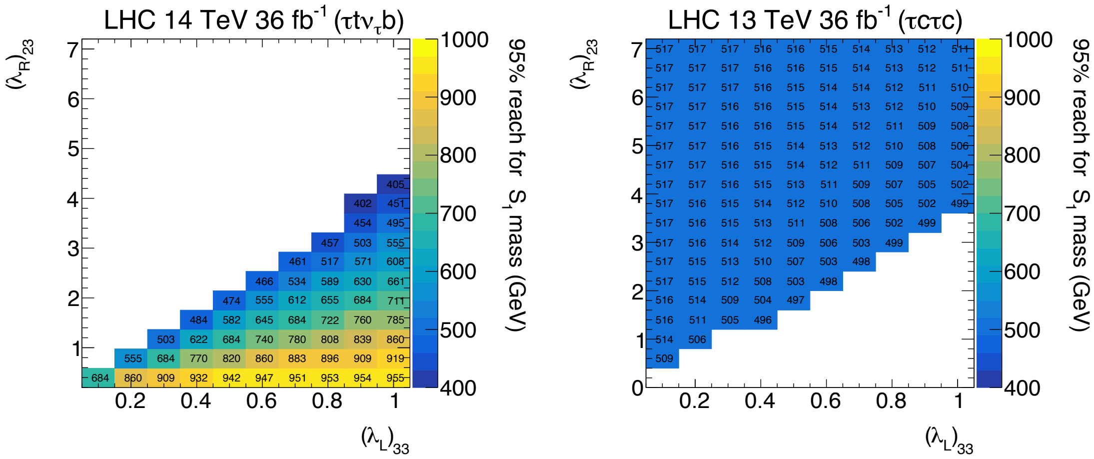

Figure 5: *Excluded values of m_{S_1} at 95% CL in the plane defined by the $(\lambda_L)_{33} - (\lambda_R)_{23}$ couplings for an integrated luminosity of 36 fb^{-1}. In the right panel the 14 TeV mixed-decay $b\nu_\tau t\tau$ analysis (described in Buttazzo et al within this proceeding volume) and on the right the rescaling of the ATLAS $b\tau b\tau$ analysis (described in the main text).*

By combining the results from the two recasts, with the currently published LHC statistics of 36 fb^{-1} a value of m_{S_1} of at least 500 GeV is (or can be) excluded at 95% CL, but significantly larger discovery potential can be expected with a dedicated $c\tau c\tau$ analysis.

To summarize, we compare in figure 6 the leptoquark mass coverage as a function of the BR for the four final states defined above for 36 fb^{-1}, where for the mixed decay $BR(S_1 \to$

$t\tau) \approx BR(S_1 \to b\nu)$ is assumed. In the searches where both leptoquarks decay in the same manner what is usually reported is the leptoquark branching fraction into a given channel, but the event rate scales with the squared of this value. Hence, for the mixed decay we plot the square of $2BR(S_1 \to b\nu)BR(S_1 \to t\tau)$. The solid lines correspond to the mass reach from the experiments and our two proposed searches, while the dashed lines correspond to our second benchmark[8]. Over most of the leptoquark mass range considered, the mixed decay $b\nu t\tau$ (dashed green) search has a higher sensitivity than the $b\nu b\nu$ (dashed blue) and the $b\tau b\tau$ (dashed red) searches. The $c\tau$ final state is only relevant for the case where the branching fraction of S_1 to other states is below about 5 %. As shown in our first benchmark, branching fractions even smaller into $b\nu$ and $t\tau$ do occur near the best fit point.

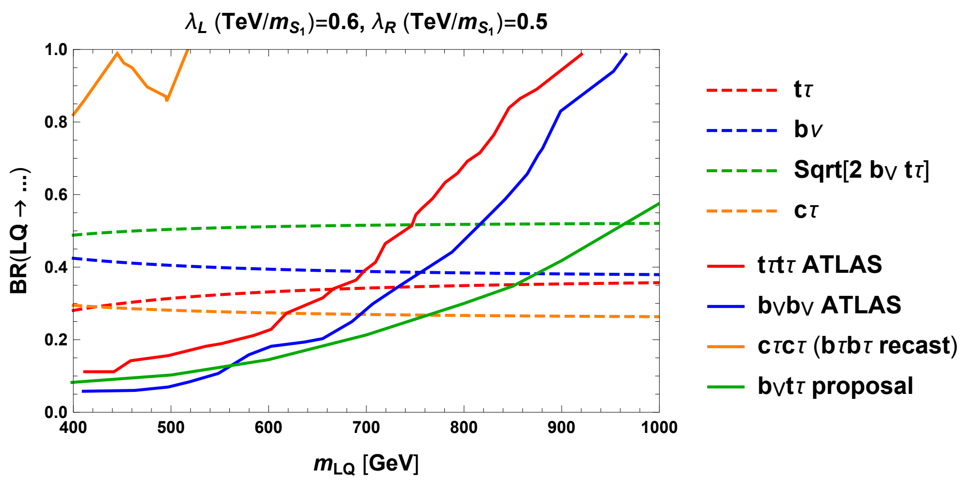

Figure 6: *Coverage of the different LQ pair searches with decays into third generation fermions. We show in dashed lines the branching ratios for the case where $x = 0.5$ and $y = 0.6$ (see main text for definition), while solid lines denote the branching ratio reach as a function of the leptoquark mass, for the $t\tau t\tau$ (red), $b\nu b\nu$ (blue), and $c\tau c\tau$ taken directly or rescaled from [32], as well as our proposed search in the $t\tau b\nu$ channel (green). For the mixed decay we plot the square of $2BR(S_1 \to b\nu)BR(S_1 \to t\tau)$, see main text for details.*

4.1.2 LQ associated production with a lepton

A single leptoquark can also be produced in association with a SM fermion, as shown in the right panel of figure 4. For our particular choice of couplings and of leptoquark charge, two single leptoquark production processes will contribute: $bg \to \nu_\tau S_1$ and $cg \to \tau S_1$. Combining with the three possible decays into SM particles shown in figure 2, one has a final state with a single b+MET (mono-b), states with a single τ + heavy quark + MET, and states with two taus and a c or a t quark.

Searches exist for the mono-b final state, but, due to the large backgrounds, and the lack of kinematic handles, we expect the sensitivity to be lower than the other channels.

The final states with a single tau and a heavy quark are addressed elsewhere in these proceedings, and will be relevant for the case where $\lambda_R \sim \lambda_L$. Given the relatively low values of λ_L compatible with the explanation of the flavour anomalies, we expect the reach in mass to

[8] In our first benchmark we only can constrain the model using the $c\tau$ analysis, hence the mass reach is about 500 GeV.

be comparable with the one from the mixed decay in pair production discussed in the previous section.

The $\tau\tau c$ final state will be the dominant channel for the case in which $\lambda_R > \lambda_L$, as the event rate scales as $\lambda_R^2 \times BR(S_1 \to c\tau)$. No search for this channel exists in the literature, but the CMS Collaboration has published a search for single leptoquark production in the $\tau\tau b$ channel [23]. As is the case for the ATLAS $b\tau b\tau$ analysis in the previous subsection, the algorithm used to tag jets from the fragmentation of b-quarks has a certain sensitivity also for jets from the fragmentation of c-quarks. Under the assumption that the kinematic acceptance of the analysis is the same for the $\tau\tau b$ and for the $\tau\tau c$ final states, the results for the $\tau\tau c$ may be obtained by a simple rescaling of the heavy-flavour tagging efficiency. In Ref. [23] they declare that they are using the combined secondary vertex algorithm at a working point with an efficiency for b-jets of approximately 60%. For this algorithm they define in Ref. [67] a medium working point with efficiency of 63% for b-jets and 12% for c-jets. We will assume the ratio of these numbers for our rescaling. The result is shown in figure 7, where the value of m_{S_1} excluded at 95% CL is shown in the plane defined by the $(\lambda_L)_{33} - (\lambda_R)_{23}$ couplings.

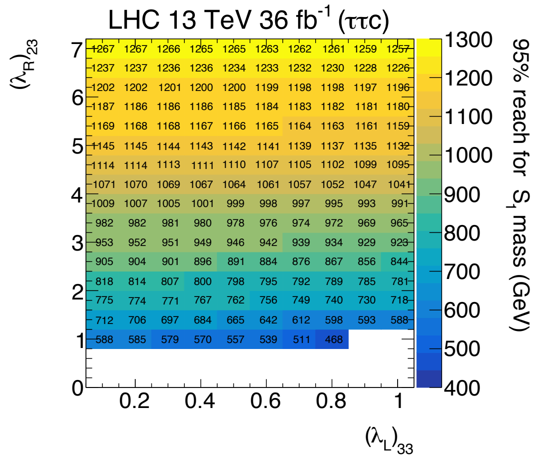

Figure 7: *Excluded values of m_{S_1} at 95% CL in the plane defined by the $(\lambda_L)_{33} - (\lambda_R)_{23}$ couplings for an integrated luminosity of 36 fb^{-1} for the CMS $\tau\tau c$ analysis as described in the text.*

Finally we compare in figure 8 the interplay of exclusions arising from pair and single leptoquark studies, where we show the 95 % C.L exclusion on λ_R as a function of m_{S_1} . For concreteness we included here only the proposed "mixed" search $b\nu t\tau$ (in red) and the $c\tau\tau$ result obtained via a recasting of the CMS study (green), and present curves using two representative values of λ_L: 0.5 (solid) and 1.0 (dashed). As previously discussed, we clearly see that the mixed search is optimal for lower values of λ_R (where the $c\tau$ final state has a comparable branching fraction with the other visible decays), while the single leptoquark search is optimal for high values of λ_R, where $c\tau$ is by far the dominant decay mode. As our benchmark points show that the flavor anomalies can be solved with either $\lambda_R \sim \lambda_L$ or $\lambda_R \gg \lambda_L$, both kind of searches are a necessary ingredient of a comprehensive campaign to probe the "leptoquark solution" of the $R_{D^{(*)}}$ anomalies.

4.2 Dark matter (missing energy) searches

Since the χ_1 particle is the lightest new particle with non-trivial SM quantum numbers, its production is strongly constrained by LHC searches, and it can only be "hidden" if χ_1 and χ_0

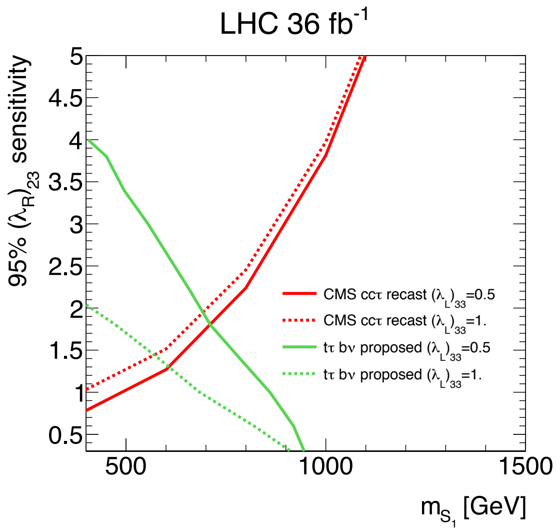

Figure 8: *Comparison of the excluded λ_R for the "mixed" $b\nu t\tau$ proposed search (green) and the $c\tau\tau$ recasting of the CMS $b\tau\tau$ study. Solid (dashed) lines denote $\lambda_L = 0.5(1.0)$.*

are close in mass. The LHC production is depicted in figure 11. Since we always assume $m_{\chi_1} < m_{S_1}$, the decay of χ_1 is entirely determined by the LQ branching ratios and the only decay channel is $\chi_1 \to S_1^*(\to lq) + \chi_0$. As shown in figure 2, χ_1 dominantly decays to $\chi_0 + c\tau$ for $\lambda_R > \lambda_L$ (third and fourth benchmarks in Table 3) or has similar BRs to $\chi_0 + c\tau$, $\chi_0 + b\nu$ and $\chi_0 + t\tau$ (first and second benchmarks) if $\lambda_R \lesssim \lambda_L$. Therefore searches for missing energy associated with jets, b-jets, tops or taus can be used to test our model.

4.2.1 b-jets plus MET searches

If $\lambda_L \gtrsim \lambda_R$ a sizeable fraction of the χ_1s produced at the LHC decay to $b\nu$ or $t\tau$. In order to constrain this scenario we re-interpret the CMS results for the sbottom simplified model $pp \to \tilde{b} + \tilde{b} \to b\tilde{\chi}_1^0 + b\tilde{\chi}_1^0$. For simplicity we assume that the decay $\chi_1 \to \chi_0 b\nu$ has similar efficiencies and the same cross-section upper limits obtained by CMS for the sbottom scenario can be applied to our model. We have used the SModelS [68] implementation of the CMS searches at 13 TeV and 35.9 fb^{-1} from Refs. [51, 52] and used it to recast the CMS bounds. The cross-sections were computed using MG5_aMC and we have applied a K-factor of 1.5 to the χ_1 pair production cross-section. The results are shown in figure 9, where we have assumed the second benchmark of Table 3 and varied m_{χ_1} and m_{χ_0}. As we can see, χ_1 masses up to 900 GeV can be excluded for sufficiently large mass gaps. However, once $m_{\chi_1} - m_{\chi_0}$ drops below 25 GeV the b-jets originating from the χ_1 decay become too soft and the search looses its sensitivity.

4.2.2 τ plus MET searches

Once $\lambda_L \lesssim \lambda_R$, the χ_1 decays are dominated by $\chi_1 \to \chi_0 + c\tau$. Although there is no LHC search which targets this final state, searches for taus plus missing energy can still be sensitive to this decay mode. Here we consider the 13 TeV ATLAS search at 139 fb^{-1} from Ref. [53], which targets final states with two taus plus missing energy and has been used to constrain the $pp \to \tilde{\tau} + \tilde{\tau} \to \tau\tilde{\chi}_1^0 + \tau\tilde{\chi}_1^0$ simplified model. Since in our model χ_1 is colored, its production cross-section is much larger than for pair production of staus and much higher masses can be

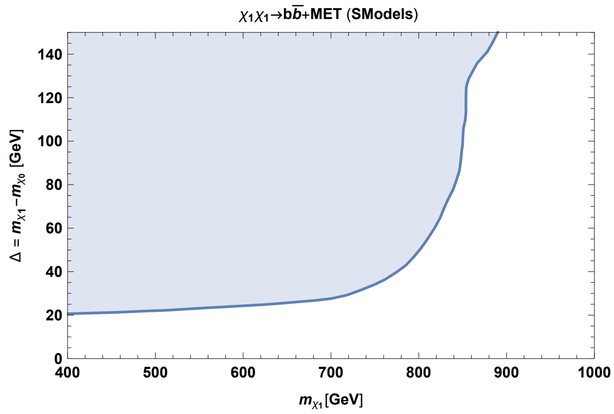

Figure 9: Region in the $m_{\chi 1} - m_{\chi 0}$ vs $m_{\chi 1}$ plane excluded by LHC searches for b-jets plus MET. The remaining model parameters are $y_\chi = 0.2$, $\lambda_L = 0.6$, $\lambda_R = 0.5$ and $m_{S_1} = 1$ TeV. The shaded region corresponds to the parameter space excluded by CMS searches for final states containing one or more b-jets and missing energy [51, 52].

tested by the analysis. The upper limits presented by ATLAS, however, are limited to $m_{\tilde{\tau}} < 450$ GeV and do not extend to the region of interest ($m_{\tilde{\chi}1} \sim$ TeV). Therefore a full recasting was done using the tools provided by CHECKMATE2 [69].[9] We also point out that since the final state considered here contains c-jets and the ATLAS analysis has a veto on b-jets, about 50% of our signal will be lost due to mis-tagging of c-jets.

Using MG5_AMC, PYTHIA 8.2 [28] and our analysis implementation in CHECKMATE2 2.0.26 we compute the 95% C.L. exclusion for the fourth benchmark model in Table 3. Once again we apply a K-factor of 1.5 for the $\chi_1\chi_1$ cross-section and vary $m_{\chi 1}$ and $m_{\chi 0}$. The result is shown in figure 10, where we see that only points with a mass gap above 80 GeV can be excluded.

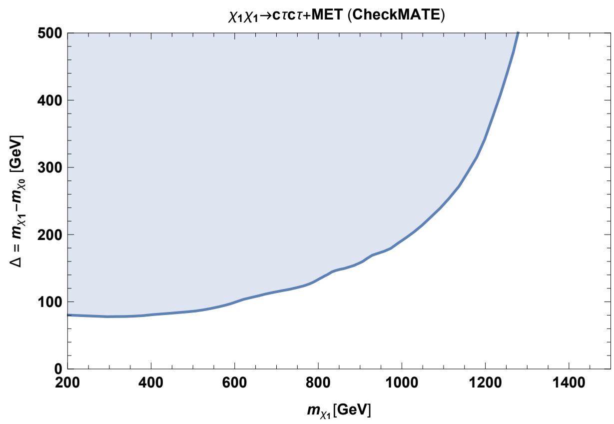

Figure 10: Region in the $m_{\chi 1} - m_{\chi 0}$ vs $m_{\chi 1}$ plane excluded by LHC searches for τ leptons plus MET. The remaining model parameters are $y_\chi = 0.2$, $\lambda_L = 0.16$, $\lambda_R = 2.0$ and $m_{S_1} = 1$ TeV. The shaded region corresponds to the parameter space excluded by ATLAS search for final states containing two hadronically decaying tau-jets and missing energy [53].

[9] The working point for the tau-tagging efficiency implemented in CHECKMATE seems to be slightly different from the one reported in Ref. [53]. Nonetheless the efficiencies obtained with our implementation are within 20%-50% of the ones obtained by ATLAS for the stau simplified model.

4.2.3 jets plut MET searches

As can be seen from figures 9 and 10, these searches lose steam once the mass gap between the parent and the daughter particle becomes small (compressed spectra). The usual strategy against a compressed spectra is to boost the system with additional radiation, leading to the mono-X (typically jet) signals. However, if the SM decay products in the $\chi_1 \to \chi_0$ are hard enough to be reconstructed (but probably not to be triggered on) the LHC sensitivity gets greatly enhanced, as shown in e.g. [70] for MSSM electroweakinos and soft-leptons. In our model this is shown in figure 11. However, the mass gap can be small enough such that the soft decay products fail to pass the reconstruction thresholds, in which case the pair production of χ particles can only be constrained by jet + MET searches. We stress that this is an unavoidable bound, that, for a given Δ, sets a lower mass on the dark sector masses. We will thus ignore here the MET searches that also include resolved (soft or hard) leptons.

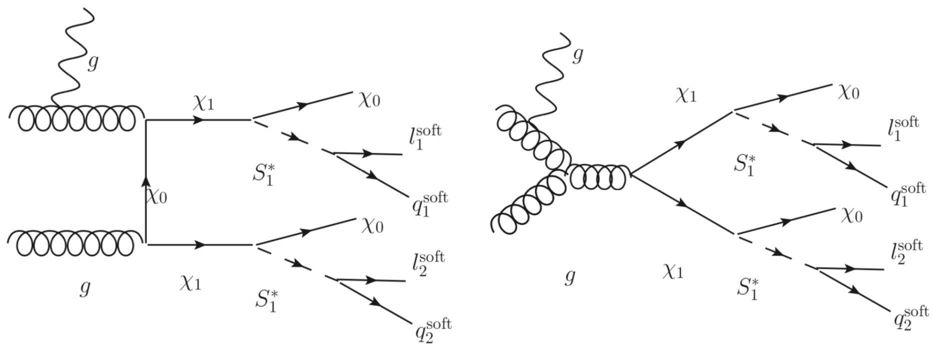

Figure 11: *Feynman diagram for monojet (plus soft leptons and quarks) signatures.*

In figure 12 we show the corresponding constraints in the $m_{\chi_1} - \Delta$ plane. In blue we show the region excluded by [55] (obtained via the MadAnalysis 5 [71,72] implementation of said study) and in orange we show the region covered by the ATLAS search of two (or more) hard jets and MET [54]. As anticipated the excluded cross section is independent of m_{χ_1} unless the spectra is compressed: the mono-jet (multi-jet) study can exclude up to 650 (750) GeV if $\Delta \gtrsim 30(10)$ GeV.

4.3 Resonant lepto-quark + MET search

The model under consideration can also be constrained by reinterpreting the results of the CMS analysis [41] specifically searching, in 77.4 fb^{-1} of LHC data, signatures of dark matter that originate from the decay of a heavy leptoquark. In this search, the signal is assumed to arise from the production of a pair of heavy scalar leptoquarks that decay differently. The first leptoquark is hence considered to decay into a muon and a jet while the second one decays into dark matter and mostly soft Standard Model states. Consequently, the searched for signal is comprised of a significant amount of missing energy, jets and a high-p_T muon.

More specifically, preselected events are required to feature at least 100 GeV of missing transverse energy and one isolated central muon candidate with a transverse momentum $p_T >$ 60 GeV and a pseudorapidity $|\eta| < 2.4$. [10] The analysis then restricts the properties of the hadronic activity in the events by constraining the centrally reconstructed jets ($|\eta| < 2.4$). The

[10] We note that our interest lies in the search with one τ lepton instead of one muon. We can, however, expect similar acceptances in the case of a leptonically decaying τ. A detailed study by the experimental collaborations

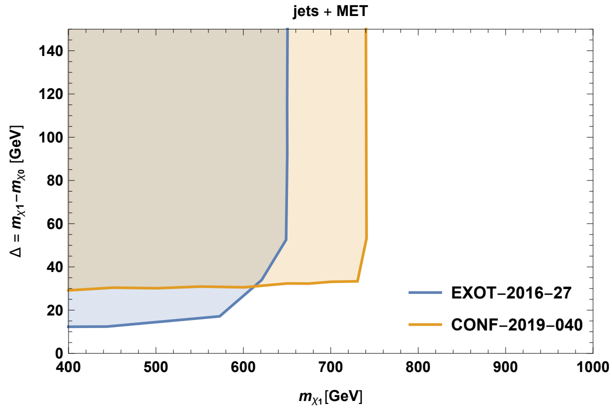

Figure 12: Region in the $m_{\chi_1} - m_{\chi_0}$ vs m_{χ_1} plane excluded by LHC studies for jets plus MET for a) more than one hard jet [54] (orange region) and b) a mono-jet search [55] (blue region) . Note that the additional model parameters $(y_\chi, \lambda_{L,R}, m_{S_1})$ do not play any relevant role here.

leading jet is hence enforced to have a transverse momentum $p_T > 100$ GeV and to be well separated, in the transverse plane, from the leading muon (by $\Delta R > 0.5$). The leading jet and leading muon are further considered to arise from the decay of a first leptoquark.

The selection then vetoes events featuring b-tagged jets, hadronic taus and electrons, as well as those featuring a second muon of electric charge opposite to the leading muon one, in which the muon pair made of these two muons is compatible with a Z-boson. Finally, the missing transverse momentum, being considered to stem from the decay of a second leptoquark, is required to be well separated in azimuth ($\Delta\phi > 0.5$) from the leading jet and muon, and the transverse mass of the system comprised of the muon and the missing energy is required to be larger than 500 GeV.

We have reimplemented this search in the MadAnalysis 5 framework [20, 72, 73], and are currently validating our reimplementation by trying to reproduce detailed cutflows kindly provided by the CMS collaboration.

With the help of our (unvalidated) reimplementation, we considering two benchmark points for which the LQ mass if fixed to 1 TeV,

$$\begin{aligned} \text{BP1}: \ m_{\chi_1} &= 400 \text{ GeV}, \ m_{\chi_0} = 380 \text{ GeV}, \\ \text{BP2}: \ m_{\chi_1} &= 600 \text{ GeV}, \ m_{\chi_0} = 200 \text{ GeV}, \end{aligned} \tag{2}$$

and where the new physics couplings are given by $\lambda_R = 2$, and $\lambda_L = 0.16$. This choice affects the LQ pair branching ratios and is motivated as to maximize the sensitivity of the CMS search. For $m_{S_1} = 1$ TeV, the total production cross section is about 3.4 fb. In table 5, we show the expected, and the observed limits on the visible cross sections at 95% CL along with the acceptance times the efficiency ($A \times \epsilon$) of the selection in the signal region The investigated scenarios are out of reach of the LHC, at least in in the channel under consideration and there is very little hope to catch up such a huge gain in sensitivity even at the HL-LHC. This is not surprising as tau-enriched final states are more relevant than muon-enriched ones in our benchmarks. This should motivate the design, by the ATLAS and/or CMS collaborations, of a similar analysis targeting the tau channel.

including also electrons and τ-leptons would be an important contribution to both the leptoquark and DM LHC search programmes.

Benchmark Point	$\sigma^{95\%}_{\rm exp}$	$\sigma^{95\%}_{\rm obs}$	$A \times \epsilon$ [%]
BP1	62.24	58.25	0.00225
BP2	112.01	104.53	0.00125

Table 5: The values of the expected, and observed visible cross sections at the 95% CL along with the acceptance times the efficiency for the two benchmark points BP1 and BP2.

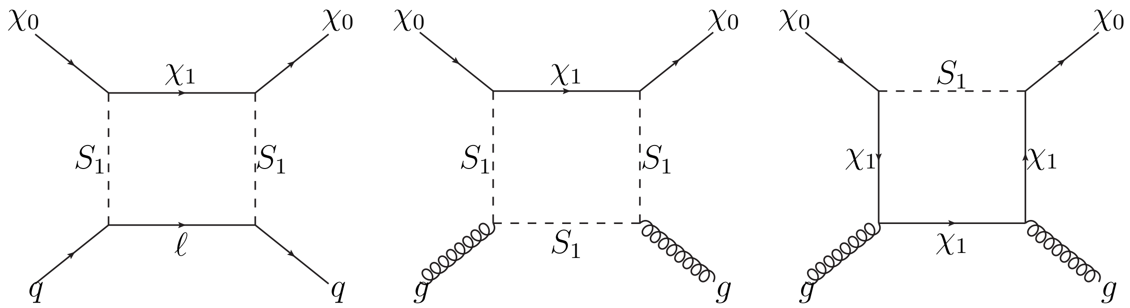

Figure 13: Feynman diagrams for the direct detection of dark matter in our model at the lowest order in perturbation theory.

5 Dark Matter constraints

In this section we study how the measured relic density and the null results of direct detection impact our model. We start by noting that the direct detection rate is one-loop suppressed (see figure 13), however given the current σ_{SI} exclusions this suppression might not be enough to discard this observable. For the relic density we consider two distinct scenarios. On one hand we study the (co)-annihilation case, as done in [40], while on the other hand we also consider the conversion-driven freeze-out (CDFO) scenario [74], also known as co-scattering [75]. The main idea behind this mechanism is that the self-annihilation of the DM candidate is negligible: the DM abundance arises instead from conversion processes within the dark sector. Hence, this scenario requires small/tiny interactions between the SM and the DM candidate (y_{DM} in our case), thus rendering the $BR(S_1 \to \chi_1\chi_0)$ negligible. This will thus affect the relevance of the collider signatures, that are discussed in detail in section 4.

5.1 Direct Detection

The scattering of χ_0 on a nucleon proceeds via 1-loop diagrams, which we show in figure 13. In the first diagram the loop include two leptoquark masses and the χ_1 mass, which are already heavy enough compared with the typical momentum transfer, so that would naively induce a mass suppression. In the second diagram one would have three leptoquark masses and a χ_1 mass, so that would be more suppressed than the diagram with three χ_1 and one S_1 in the loop.

Integrating out the heavy degrees of freedom χ_1 and S_1, we can obtain a rough estimate for the Wilson coefficient of the rightmost diagram, finding that $y_\chi \lesssim 1$. This result implies that direct detection constraints have an impact on our parameter space, and hence a complete 1-loop calculation taking into account all possible diagrams and interference effects is incumbent and is left for future work [11].

[11]Such a calculation was carried out for a similar model [76], however in that case S_1 is a t-channel mediator

5.2 Relic Density

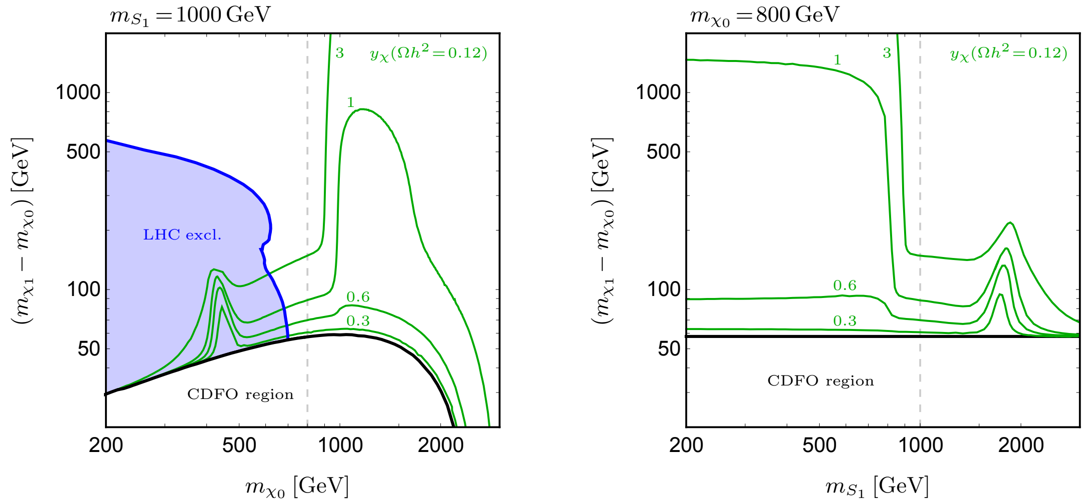

Figure 14: Parameter space satisfying $\Omega h^2 = 0.12$. The solid black line denotes the boundary between the standard freeze-out and conversion-driven freeze-out (CDFO) regime. The thin green curves denote contours of constant coupling y_χ. We also overlay the envelope of the missing energy searches (blue region) discussed in the previous section.). *Left panel:* Plane spanned by $m_{\chi 0}$ and $(m_{\chi 1} - m_{\chi 0})$ while fixing $m_{S_1} = 1000\,$GeV. *Right panel:* Plane spanned by m_{S_1} and $(m_{\chi 1} - m_{\chi 0})$ while fixing $m_{\chi 0} = 800\,$GeV. We choose $\lambda_L = 0.6\, m_{S_1}/\text{TeV}$ and $\lambda_L = 0.5\, m_{S_1}/\text{TeV}$. The vertical grey dashed line in the left panel indicates the fixed mass value in the right panel and vice versa.

In figure 14 we display contours of constant y_χ satisfying the correct relic abundance, $\Omega h^2 \simeq 0.12$ [77], computed with MICROMEGAS [44]. We consider two slices of the parameter space. In the left panel we fix $m_{S_1} = 1000\,$GeV and $\lambda_L = 0.6, \lambda_L = 0.5$ (second benchmark point in table 3), which renders it safe from the leptoquark searches described in section 4. In the right panel we fix $m_{\chi 0} = 800\,$GeV and m_{S_1} while keeping $\lambda_L = 0.6\, m_{S_1}/\text{TeV}$ and $\lambda_L = 0.5\, m_{S_1}/\text{TeV}$ consistent with the flavour anomalies.

As mentioned above, cosmologically allowed parameter space falls into two main classes: The standard thermal freeze-out regime with $y_\chi \sim \mathcal{O}(1)$ and the CDFO regime, residing above and below the thick black curve, respectively. For the latter the required couplings are small such that the decay of coannihilating partner is typically non-prompt [74]. In the standard freeze-out regime co-annihilations are important. The y_χ contours show two prominent features. The one at $m_{\chi 0} \sim m_{S_1}/2$ arises from resonantly enhanced coannihilation via an s-channel LQ, while the one at $m_{\chi 0} \sim m_{S_1}$ is due to the opening of DM pair-annihilation into a pair of LQs. Qualitatively, the phenomenology is very similar to the one of the top-philic charge parent model as studied in [78]. Note that for $m_{\chi 0} < m_{S_1}/2$ loop-induced DM annihilation into gluons can become important [78] which is, however, neglected here.

We overlay on top of these curves the "envelope" of the missing energy searches, which clearly disfavors low masses except for small mass splittings, where solutions in the CDFO regime can be found. Here, the applicability of LHC searches depends on the lifetime of the metastable χ_1 and is investigated elsewhere. For non-compressed mass spectra limits from the LHC require $m_{\chi_1} \gtrsim 750$ GeV.

(instead of s-channel), and there is no χ_1 particle.

Note that in the CDFO region the S_1 branching fractions into the dark sector would be negligible, and the invisible decay of S_1 would not be seen at colliders. The only handle into the dark world are the χ_1 searches (note that this is also true for the low m_{χ_1} region with compression). In the thermal freeze-out case one can have, besides the LQ, missing energy and direct detection searches, also information from the resonant leptoquark plus missing energy searches, thus allowing to firmly establish a connection between the flavor anomalies and the dark sector.

5.3 Indirect Detection

In general indirect detection constitutes an important probe of the self-annihilating nature of DM. In the considered model annihilation today dominantly takes place either via the $2 \to 2$ process $\chi_0\chi_0 \to S_1 S_1$, if $m_{S_1} < m_{\chi_0}$, or via $2 \to 4$ or loop-induced $2 \to 2$ processes otherwise. In the first case the leading contribution is p-wave suppressed and hence the corresponding cross sections are small. The same is true for the $2 \to 4$ process which is suppressed by the off-shell S_1 propagator. Points where annihilation dominantly proceeds via these processes are, hence, not expected to be challenged by current or upcoming indirect detection searches.[12] If, in contrast, annihilation in the early Universe proceeds predominantly via the loop-induced $2 \to 2$ processes, requiring large y_χ, the situation might change and the corresponding cross section today might be sizeable. In particular, the signature of mono-chromatic gamma lines, appearing at the same loop-level, can be a promising search strategy given higher sensitivity [82, 83]. However, as the region $m_{S_1} < m_{\chi_0}$ is not the prime focus of this study, we leave a detailed study of this case for future work.

6 Conclusions and Outlook

The charged-current flavor anomalies hint at the present of leptoquarks near or at the TeV scale. Here we have studied the connection between these models and dark matter, which necessarily requires to add new particles and couplings. Employing a simplified model with only 6 parameters we have scanned the parameter space vis-a-vis the aforementioned flavor anomalies, relic density, direct detection and LHC constraints.

We have seen that when taken all these constraints simultaneously one is left with two possible scenarios: either the dark sector couples to the leptoquark mediator with a similar strength than the one required from taking the $R_{D^{(*)}}$ anomaly at face-value, which then implies a traditional freeze-out scenario to account for the current abundance of dark matter, or the leptoquark couples faintly to the dark sector, which in turn implies that the dark matter abundance arises from the conversion-driven freeze-out (co-scattering) mechanism. In the second scenario the leptoquark branching fraction into the dark sector is negligible, and thus the phenomenology will consist of seemingly disconnected leptoquark “anomaly-inspired" and traditional missing energy + X signatures. In the latter case, depending on the “compression" between the dark sector particles, one can resolve the leptons and quarks from the $S_1 \to \chi_1\chi_0 \to lq\chi_0\chi_0$ decay chain, which would then allow to establish a firm connection between both new physics signals. In the case where the branching fraction into the dark sector is non-negligible, then the strongest indication of the leptoquark-dark matter connection is through the pair production of

[12] For instance, choosing $m_{\chi_0} = 800\,\text{GeV}$, $m_{\chi_1} = 1000\,\text{GeV}$, $y_\chi = 0.71$ (obeying $\Omega h^2 \simeq 0.12$) and $m_{S_1} = 500$ GeV, (according to benchmark point 1) yields a annihilation cross section $\langle\sigma v\rangle_0 \simeq 3 \times 10^{31}\,\text{cm}^3/\text{s}$, way below current limits from gamma rays [79] or cosmic rays [80]. Note that the corresponding spectra (computed with MADDM [81]) are similar to the one for annihilation into $b\bar{b}$ considered as a benchmark in these analyses.

leptoquarks with one decaying into the dark sector and another one into hard leptons and quarks. Since this search is only being conducted currently by the CMS collaboration, we encourage the ATLAS collaboration to undertake this key study for a comprehensive dark matter program going beyond the mere annihilation into singlet final states.

Along this work we have pointed out the existence of three important holes in the campaign to optimally cover the leptoquark parameter space. On one side we have noted that for leptoquarks decaying into the third generation fermions (almost) exclusively, a search in the $b\nu t\tau$ should be added to the existing ones looking into $b\nu b\nu$ and $t\tau t\tau$, where one can benefit from a larger branching fraction, and devise cuts to keep the background under control, which we have demonstrated with a simple analysis. On the other side, noting that the solutions to the $R_{D^{(*)}}$ anomalies involve larger couplings connecting second generation quarks with third generation leptons, we advocate to study the $c\tau c\tau$ final state, and if possible and depending on the c-tagging efficiencies, also include the mixed cases, e.g $c\tau t\tau$ or $b\nu c\tau$ final states. Finally, it is also important to include single leptoquark searches decaying largely into $c\tau$, namely study the $c\tau\tau$ final state.

Our results show that the exploration of common solution to the $R_{D^{(*)}}$ anomalies and the dark matter puzzle is an interesting research avenue, and we thus plan to expand the preliminary results presented here into a comprehensive study of this model, vis-a-vis current constraints and also considering future projections of LHC and direct detection coverage.

Acknowledgements

W would like to thank the organizers of the Les Houches “Physics at TeV Colliders" 2019 Session for setting up an interesting workshop and providing an ideal atmosphere for scientific exchange. The work of A.L. was supported by the São Paulo Research Foundation (FAPESP), project 2015/20570-1. J.H. acknowledges support from the F.R.S.-FNRS, of which he is a postdoctoral researcher. The work of D.S. is based upon work supported by the National Science Foundation under Grant No. PHY-1915147.